RSC Advances

ROYAL SOCIETY OF CHEMISTRY

www.rsc.org/advances

Photosensitive self-assembling materials as functional dopants for organic photovoltaic cells

Alexej Bubnov[1]*, Agnieszka Iwan[2+], Martin Cigl[1], Bartosz Boharewicz[2], Igor Tazbir[2], Kamil Wójcik[2], Andrzej Sikora[2], Věra Hamplová[1]

[1]*Institute of Physics, The Czech Academy of Sciences, Na Slovance 1999/2, 182 21 Prague, Czech Republic; *e-mail: bubnov@fzu.cz*

[2]*Electrotechnical Institute, Division of Electrotechnology and Materials Science, M. Sklodowskiej-Curie 55/61 Street, 50-369 Wroclaw, Poland, [+]e-mail: a.iwan@iel.wroc.pl*

Abstract

New photosensitive liquid crystalline compounds with a specific molecular structure have been designed in order to use them as functional dopants for the organic photovoltaic devices. The main idea is to establish the effect of doping on the bulk-heterojunction solar cell properties and characteristics. As a part of basic characterisation, the self-assembling behaviour of three new organic compounds has been determined. The resulting photovoltaic devices with P3HT:PCBM active layer doped by the designed photosensitive materials were investigated by UV-Vis spectroscopy, electrochemical measurements, cyclic voltammetry experiments, AFM surface morphology studies and impedance spectroscopy. The obtained results are summarised and discussed in terms of power conversion efficiency improvement considering the specific chemical structure of the compounds used as functional dopants and the annealing temperature of an active layer. The molecular structure of compounds used as dopant has a strong effect on the value of short circuit current density. However, no significant effect of the dopant in P3HT:PCBM active layer on the open circuit voltage and fill factor has been found.

Keywords: photosensitive composite; photovoltaics; azo materials; liquid crystal; bulk heterojunction solar cells; self-assembling material

1. Introduction

Design of the light-harvesting and energy-converting systems belongs to one of the most highlighted fields of modern research [1-2]. Tuning and increasing the power conversion efficiency (PCE) of the organic photovoltaic (OPV) cells remains an actual and highlighted topic though several approaches has been successfully developed during the last years. Despite recent advances in solid-state photovoltaic devices [3-5], bulk-heterojunction (BHJ) organic photovoltaics [6] continue to be an attractive low-cost renewable energy technology. The main reason for the prosperity is that the OPVs are enable roll-to-roll printing of environmentally friendly, mechanically flexible and cost-effective photovoltaic devices [7].

Recent developments in OPV device design targets using the self-assembling materials as specific functional dopants [8-12]. There are numerous attempts to use the extraordinary properties of self-assembling materials, both the low molar mass and macromolecular ones [13-14], for improvement of the OPV devices [15-27]. Switchable liquid crystalline (LC) coatings placed on top of the photovoltaic layer might also considerably increase the OPV device efficiency [28]. The self-assembling properties of the nematic LC gels allow an alternative way to generate a vertically separated and distributed interface between electron donating and accepting materials that improves the OPV efficiency [29]. Further crosslinking of LC gels results in additional improvement of the thermal stability and allows photolithographic pattering [29]. Actual developments in organic solar cell design suggest exploitation of new low molar mass organic compounds as functional dopants to the active layers of photovoltaic devices. The increase of the OPV performance can be reached by means of morphology control of active layers, investigation of the intermolecular interactions and material's miscibility [30-32].

As it has been discussed above, beyond the application of the low molar mass LC materials for flat-panel displays and non-linear optical systems [33-35], self-assembling materials can be very useful for the improvement of the organic photovoltaic devices. During last decades many non-chiral and chiral liquid crystalline compounds of quite different molecular structure have been designed [36-40]. Numerous low molar mass compounds [41-47], polymeric side-chain compounds [48-54] and even dendrimers [55] with different structure, molecular shape, symmetry and consequently with different mesomorphic behaviour have been designed as self-assembling materials possessing extraordinary thermal, optic and structural properties. It is quite common that compounds of different molecular shape and structure can exhibit one mesophase or a sequence of mesophases characterized by a different orientational order like nematic, smectic, columnar, etc. Chiral liquid crystalline materials, specifically those derived

from the lactic acid, can form a broad variety of mesophases such as chiral nematic but also various smectic phases in which the molecules are self-assembled in layers (i.e. nano-layered phases). Due to their smart advantages with respect to other conventional materials [35, 37, 41, 45, 56] lactic acid derivatives can be prosperously used as a smart dopants for OPV devices [57-58]. An induction of polymerizable groups at one of the alkyl terminal chains [37-39, 48, 52-53] or incorporation of a photosensitive azo group in the molecular core [39-40, 48, 59-62] can strongly increase the potential functionality of this class of chiral LC materials. As a result of their properties meeting the terms of specific demands, lactic acid derivatives are actively used as strongly effective and reasonably cheap dopants for tuning properties of the resulting mixture [37, 42, 63-64] or advanced nanocomposite systems [65-66].

Recently an effect for improving the PCE of the organic solar cells by photosensitive self-assembling materials doping has been established [57-58]. It has been shown that thermal annealing within the mesophase temperature range can remove defects, optimize the morphology of the LC doped active layer of the OPV device, and hence, in special cases, might be responsible for the PCE increase [57]. However, the relationship between the PCE improvement and the molecular structure of the LC functional dopants is still not clear enough. The main objective of this work is to contribute to better understanding the selection rules for the specific organic molecular structures to be used as functional dopants for the improvement of the PCE of the OPV devices. Specifically the work is aimed to find a synergy between liquid crystalline azo-compounds and polymer solar cells to produce smart BHJ devices and to study the effect of LC azo-compounds on their photovoltaic parameters.

Improvement of the active layer micro-structure order as a consequence of intermolecular interactions within the temperature range of LC mesophase is expected to enrich photoelectric properties of polymer devices [67].

2. Design and characterisation of new photosensitive LC materials

Design and synthesis details of new photosensitive compounds used as functional dopants for OPV cells are described in this section together with basic characterisation of the material properties, namely the confirmation of the molecular structure by ^{1}H NMR, ^{13}C NMR, etc. Molecular structures of photosensitive dopants (see Fig. 1) were derived from the structures of previously designed materials [57-58]. Two lateral methoxy groups were introduced to the structure in order to enhance the absorption in the visible region of the UV-Vis spectra. Lateral substitution is also a good tool for modification of HOMO-LUMO energy levels. However, such bulky substituents placed on the molecular core usually results in loss of LC

properties. In order to increase the length/width ratio of the molecule and to obtain mesogenic materials, an induction of extra aromatic ring to the molecular core of two specific dopants (denoted as **DOBP**, **DOLZ** – see Fig. 1) has been suggested and realised.

2.1. Synthesis

Scheme of the synthesis route for new photosensitive liquid crystalline compounds is presented in Figure 1. All initial materials, reagents and solvents were purchased from Sigma-Aldrich or Acros Organics. Intermediates **8** and **9** were synthesized by known procedures [68-69] ^{1}H NMR spectra were recorded on Varian Gemini 300 HC instrument; deuteriochloroform ($CDCl_3$) and hexadeuteriodimethyl sulfoxide (DMSO-d_6) were used as solvents and signals of the solvent served as internal standard. Chemical shifts (δ) are given in ppm and *J* values are given in Hz. Signals were identified using APT, gCOSY and gHMBC experiments. For all azo compounds, only spectra of *E*-isomer are given. The purity of all final compounds were checked by HPLC analysis (high-pressure pump ECOM Alpha; column WATREX Biospher Si 100, 250 × 4 mm, 5 μm; detector WATREX UVD 250) and were found to be >99.8 %. Column chromatography was carried out using Merck Kieselgel 60 (60–100 μm).

[inset Figure 1 about here]

2.1.1. *N-(4-(Oktyloxy)phenyl)acetamide* (2)

A mixture of 4-acetamidophenol (**1**) (15.0 g, 0.10 mol), 1-bromooctane (15.30 g, 0.11 mol) and potassium hydroxide (6.15 g, 0.11 mol) in aqueous ethanol (80%, 400 ml) was heated under reflux for 12 h. After cooling to room temperature, the solution was poured into water (1000 ml). Precipitated *N*-(4-(octyloxy)phenyl)acetamide was filtered off, washed with water and recrystallized from ethanol. Yield 25.80 g (98 %), white solid.

^{1}H NMR ($CDCl_3$) δ for **(2)**: 7.35 (2 H, d, *J* = 9.1, H-2, H-6); 6.83 (2 H, d, *J* = 9.1, H-3, H-5); 3.90 (2 H, t, *J* = 6.3, CH_2O); 2.14 (3 H, s, CH_3CO); 1.75 (2 H, quin., *J* = 7.1, C**H**$_2$$CH_2O$); 1.2 - 1.5 (8 H, m, $(CH_2)_4$), 0.88 (3 H, t, *J* = 7.0, C**H**$_3$$CH_2$).

2.1.1. 4-(Oktyloxy)phenylammonium-hydrogensulphate (3).

N-(4-octyloxyphenyl)acetamide (25.80 g,97.96 mmol) was suspended in diluted sulphuric acid (250 ml, 1:1) and refluxed, until the solid was completely dissolved. After cooling to

room temperature, the precipitate was filtered off, washed with water and recrystallized from aqueous ethanol (70%) to yield white solid **3** (30.0 g, 95 %).

^{1}H NMR (DMSO-d_6) δ for **(3)**: 7.43 (2 H, d, J = 9.1, H-2, H-6); 7.20 (2 H, d, J = 9.1, H-3, H-5); 3.96 (2 H, t, J = 6.3, CH_2O); 1.73 (2 H, quin. J = 7.1, C**H**$_2$$CH_2O$); 1.2 - 1.5 (8 H,m, $(CH_2)_4$), 0.86 (3 H, t, J = 7.0, C**H**$_3$$CH_2$).

2.1.3. *3′,5′-Dimethoxy-4′-((4-(octyloxy)phenyl)diazenyl)phenol* (4)

A solution of sodium nitrite (5.0 g, 0.07 mol in 5 ml of water) was added dropwise to a suspension of 4-(octyloxy)phenylammonium-hydrogensulphate (**3**) (15.0 g, 46.96 mmol) in glacial acetic acid (50 ml), keeping the temperature below 5 ºC. Reaction mixture was stirred for another 30 min and then solid urea was added to eliminate the excess of nitrous acid. The resulting solution was added portion-wise with stirring to the mixture of 3,5-dimethoxyphenol (6.20 g, 0.05 mol) and sodium hydroxide (72.0 g, 1.80 mol) in water (200 ml). The temperature of the reaction was kept below 10 °C by ice water bath. After the last portion of diazonium salt solution, the reaction mixture was stirred for 1 hour. A red solid precipitated, was filtered off and washed with HCl (100 ml, 1 : 5) and with water. Crude product was purified by crystallization from ethanol. Yield 11.60 g (64 %).

^{1}H NMR (DMSO-d_6) δ ppm for **(4)**: 8.30 (1 H, s, OH), 7.68 (2 H, d, J = 8.8, H-2, H-6), 7.05 (2 H, d, J = 8.8, H-3, H-5), 6.20 (2 H, s, H-2′, H-6′), 4.02 (2 H, t, J = 6.6, OCH_2), 3.81 (6 H, s, 2 × OCH_3), 1.71 (2 H, quin. J = 7.1, C**H**$_2$$CH_2O$), 1.14 – 1.55 (10 H, m, $(CH_2)_5$), 0.85 (3 H, t, J = 6.5, CH_2C**H**$_3$).

^{13}C NMR (DMSO-d_6) δ ppm for **(4)**: 159.96 (C-1′), 156.94 (C-4), 155.28 (C-3′, C-5′), 143.13 (C-1), 124.02 (C-4′), 122.49 (C-2, C-6), 114.94 (C-3, C-5), 93.79 (C-2′, C-6′), 67.91 (CH_2O), 56.44 (OCH_3), 31.19 (**C**$H_2CH_2CH_3$), 28.69 (**C**H_2CH_2O), 28.58 – 28.61 (m, 2 × $(CH_2)_2$), 25.44 (**C**$H_2CH_2CH_2O$), 22.03 (**C**H_2CH_3), 13.91 (CH_2**C**H_3).

2.1.4. *(S)-1-(hexyloxy)-1-oxopropan-2-yl 4-formylbenzoate* (6)

A mixture of 4-formylbenzoic acid (**5**) (15.80 g, 0.10 mol) and (*S*)-hexyllactate (17.40 g, 0.10 mol) was dissolved in a mixture of dichloromethane and THF (200 + 200 ml). Dicyclohexylcarbodiimide (21.70 ml (0.11 mol) and 4-(*N,N*-dimethylamino)pyridine (1.30 g, 0.01 mol) was added and the mixture was stirred for 24 h at room temperature. Precipitated dicyclohexylurea was filtered off and the filtrate washed with HCl (150 ml, 1 : 15) and water.

Organic layer was dried with anhydrous sodium sulphate. Removal of the solvent under reduced pressure yielded benzoate **7** as a colourless viscous liquid (28.80 g, 94 %) Product was used in the next step without further purification.

^{1}H NMR ($CDCl_3$) δ ppm for **(6)**: 10.11 (1 H, s, CHO) 8.25 (2 H, d, *J* = 8.8, H-3, H-5), 7.97 (2H, d, *J* = 8.8, H-2, H-6), 5.37 (1 H, q, *J* = 7.1, CH*), 4.11 - 4.24 (2 H, m, COOC**H**$_2$), 1.57 - 1.71 (5 H, m, C**H**$_3$CH*, $COOCH_2C$**H**$_2$), 1.16 - 1.42 (6 H, m, $(CH_2)_3$), 0.88 (3 H, t, *J* = 6.7, CH_2C**H**$_3$).

2.1.5. *(S)-4-(((1-(hexyloxy)-1-oxopropan-2-yl)oxy)carbonyl)benzoic acid* (7)

The solution of potassium permanganate (14.5 g, 0.09 mol) in water (100 ml) at cca 50 °C was added in 8 portions every 15 min to the agitated solution of 4-formylbenzoate **6** (28.80 g, 0.09 mol) in pyridine, cooled to - 10°C by the ice-salt bath. After the last addition, the mixture was allowed to stand overnight at - 20°C and then it was slowly added to the mixture of of conc. HCl (150 ml) in the ice-cold water (500 ml). Resulting suspension was neutralized by the additional amount of concentrated HCl (50 ml) and filtered through the suction with a pad of celite. Filtered solid was boiled with acetone (200 ml) and filtered again. Filtrate was dried with anhydrous sodium sulphate. Evaporation of the acetone yielded crude **7** which was recrystallized from heptane. Yield 26.40 g (91 %), white solid, m.p. 69 – 70°C.

^{1}H NMR ($CDCl_3$) δ for **(7)**: 8.19 (4 H, s, Ar-H), 5.36 (1 H, q, *J* =7.1, CH*), 4.12 - 4.24 (2 H, m, COOC**H**$_2$), 1.57 - 1.71 (5 H, m, C**H**$_3$CH*, $COOCH_2C$**H**$_2$), 1.16 - 1.42 (6 H, m, $(CH_2)_3$), 0.88 (3 H, t, *J* = 6.7, CH_2C**H**$_3$).

2.1.6. *(S,E)-3′,5′-dimethoxy-4′-((4-(octyloxy)phenyl)diazenyl)phenyl (1-(hexyloxy)-1-oxopropan-2-yl) terephthalate* (DOTL)

Phenol **4** (3.0 g, 7.95 mmol) and benzoic acid **7** (2.6 g, 8.07 mmol) were dissolved in dry dichloromethane (120 ml) and the resulting solution was cooled to 0 °C. Then dicyclohexylcarbodiimide (1.70 g, 8.24 mmol) and 4-(*N,N*-dimethylamino)pyridine (0.08 g, 0.65 mmol) were added. The mixture was stirred for 6 h and then the precipitated dicyclohexylurea was filtered off. Solvent was removed under reduced pressure and the crude product purified by column chromatography on silica (dichloromethane-acetone, 98 : 2). Further recrystallization from hexane yielded 4.92 g (90 %) of **DOTL**.

^{1}H NMR (300 MHz, CDCL3) δ ppm for **DOTL** compound: 8.26 (4 H, m, H-2′′, H-3′′, H-5′′, H-6′′), 7.90 (2 H, d, *J* = 8.8, H-2, H-6), 7.00 (2 H, d, *J* = 8.8, H-3, H-5), 6.62 (2 H, s, H-2′, H-

6′), 5.38 (1 H, q, J = 7.0, CH*), 4.20 (2 H, m, CH*COOC**H**$_2$), 4.05 (2 H, t, J = 6.6, CH_2O), 3.85 (6 H, s, 2 × OCH_3), 1.83 (2 H, quin. J = 7.1, C**H**$_2$$CH_2O$), 1.67 (5 H, m, C**H**$_3$CH*, $COOCH_2$C**H**$_2$), 1.20 – 1.55 (16 H, m, 8 × CH_2), 0.89 (6 H, m, 2 × CH_2C**H**$_3$).

^{13}C NMR (75 MHz, DMSO-d_6) δ ppm for **DOTL** compound: 170.50 (CH***C**OO), 164.97 (**C**OOCH*), 164.03 (COOAr), 161.75 (C-4), 152.87 (C-3′, C-5′), 151.13 (C-1′), 147.64 (C-1), 134.05 (C-4′′), 133.45 (C-1′′), 131.79 (C-4′), 130.13 (C-2′′, C-6′′), 129.99 (C-3′′, C-5′′), 124.51 (C-2, C-6), 114.61 (C-3, C-5), 99.22 (C-2′, C-6′), 69.68 (CH*), 68.38 (CH_2O), 65.65 (CH*COO**C**H_2), 56.60 (Ar(OCH_3)$_2$), 31.79 (**C**$H_2CH_2CH_3$-b), 31.30 (**C**$H_2CH_2CH_3$-a), 29.32 (**C**$H_2(CH_2)_3O$), 29.21 (**C**$H_2(CH_2)_2CH_3$), 29.17 (**C**H_2CH_2O-b), 28.44 (**C**H_2CH_2O-a), 25.99 (**C**$H_2(CH_2)_2O$-b), 25.41 (**C**$H_2CH_2CH_2O$-a), 22.63 (**C**H_2CH_3-b), 22.46 (**C**H_2CH_3-a), 17.16 (CH***C**H_3), 14.05 (CH_2**C**H_3-b), 13.95 (CH_2**C**H_3-a).

2.1.7. *(E)-3′,5′-dimethoxy-4′-((4-(octyloxy)phenyl)diazenyl)phenyl 4′′′-(dodecyloxy)-[1′′,1′′′-biphenyl]-4′′-carboxylate* (DOBP)

Phenol **4** (1.30 g, 3.36 mmol) and acid **8** (1.30 g, 3.40 mmol) were dissolved in dry dichloromethane (120 ml) and the resulting solution was cooled to 0 °C. Then dicyclohexylcarbodiimide (0.80 g, 3.88 mmol) and 4-(*N,N*-dimethylamino)pyridine (0.04 g, 0.33 mmol) were added. The mixture was stirred for 10 h and then the precipitated dicyclohexylurea was filtered off. Solvent was removed under reduced pressure and the crude product purified by column chromatography on silica (dichloromethane-acetone, 99.5 : 0.5). Further recrystallization from hexane and methanol yielded 2.23 g (88 %) of **DOBP**.

^{1}H NMR (300 MHz, CDCL3) δ ppm for **DOBP** compound: 8.25 (2 H, d, J = 8.2, H-3′′, H5′′), 7.90 (2 H, d, J = 8.8, H-2, H-6), 7.72 (2 H, d, J = 8.2, H-2′′, H-6′′), 7.62 (2 H, d, J = 8.8, H-2′′′, H6′′′), 7.01 (4 H, m, H-3, H-5, H-3′′′, H-5′′′), 6.62 (2 H, s, H-2′, H-6′), 4.04 (4 H, m, 2 × CH_2O), 3.85 (6 H, s, 2 × CH_3O), 1.83 (4 H, m, 2 × C**H**$_2$$CH_2O$), 1.17 – 1.56 (28 H, m, 14 × CH_2), 0.90 (6 H, m, 2 × CH_2C**H**$_3$).

^{13}C NMR (75 MHz, CDCL3) δ ppm for **DOBP** compound: 164.88 (COO), 161.64 (C-4), 159.59 (C-4′′′), 152.86 (C-3′, C-5′), 151.55 (C-1′), 147.59 (C-1), 146.11 (C-1′′), 131.80 (C-1′′′), 131.34 (C-4′), 130.73 (C-3′′, C-5′′), 128.37 (C-2′′′, C-6′′′), 127.18 (C-4′′), 126.60 (C-2′′, C-6′′), 124.49 (C-2, C-6), 114.95 (C-3′′′, C-5′′′), 114.55 (C-3, C-5), 99.24 (C-2′, C-6′), 68.33 (CH_2O-b), 68.14 (CH_2O-a), 56.55 (2 × OCH_3), 31.91 (**C**$H_2CH_2CH_3$-b), 31.80 (**C**$H_2CH_2CH_3$-a), 29.61 (5 × CH_2), 29.39 (**C**$H_2(CH_2)_3O$-b), 29.35 (**C**$H_2(CH_2)_3O$-a), 29.23

(**C**$H_2(CH_2)_2CH_3$), 29.16 (2 × **C**H_2CH_2O), 26.02 (**C**$H_2CH_2CH_2O$-b), 25.99 (**C**$H_2CH_2CH_2O$-a), 22.69 (**C**H_2CH_3-b), 22.65 (**C**H_2CH_3-a), 14.13 (2 × CH_2**C**H_3).

2.1.8. *(S,E)-3′,5′-dimethoxy-4′-((4-(octyloxy)phenyl)diazenyl)phenyl 4′′′-((2-(octyloxy)propanoyl)oxy)-[1′′,1′′′-biphenyl]-4′′-carboxylate* (DOLZ)

Phenol **4** (1.80 g, 4.66 mmol) and acid **8** (1.90 g, 4.77 mmol) were dissolved in dry dichloromethane (120 ml) and the resulting solution was cooled to 0 °C. Then dicyclohexylcarbodiimide (1.0 g, 4.85 mmol) and 4-(*N,N*-dimethylamino)pyridine (0.06 g, 0.49 mmol) were added. The mixture was stirred for 10 h and then the precipitated dicyclohexylurea was filtered off. Solvent was removed under reduced pressure and the crude product purified by column chromatography on silica (dichloromethane-acetone, 98 : 2). Further recrystallization from hexane and methanol yielded 2.39 g (85 %) of **DOLZ**.

^{1}H NMR (300 MHz, $CDCl_3$) δ ppm for **DOLZ** compound: 8.29 (2 H, d, *J* = 8.2, H-3′′, H5′′), 7.90 (2 H, d, *J* = 8.8, H-2, H-6), 7.71 (4 H, m, H-2′′, H6′′, H-2′′′, H6′′′), 7.25 (4 H, d, *J* = 8.5, H-3, H-5), 7.00 (2 H, d, *J* = 8.8, H-3′′′, H-5′′′), 6.62 (2 H, s, H-3, H-5), 4.23 (1 H, q, *J* = 6.7, CH*), 4.05 (2 H, *J* = 6.5, CH_2O), 3.85 (6 H, s, 2 × CH_3O), 3.72 (2 H, dt, *J* = 8.8, 6.6, C**H**^{a}H^{b}OCH*), 3.52 (1 H, dt, *J* = 8.8, 6.7, CH^a**H**^{b}OCH*), 1.83 (2 H, quin. *J* = 6.8, C**H**$_2$$CH_2O$-a), 1.66 (5 H, m, C**H**$_3$CH*, $COOCH_2$C**H**$_2$), 1.19 – 1.54 (20 H, m, 10 × CH_2), 0.89 (6 H, m, 2 × CH_2**C**H_3).

^{13}C NMR (75 MHz, CDCL3) δ ppm for **DOLZ** compound: 172.04 (CH***C**OO), 164.71 (ArCOO), 161.68 (C-4), 152.87 (C-3′, C-5′), 151.45 (C-1′), 150.68 (C-4′′′), 147.59 (C-1), 145.47 (C-1′′), 137.63 (C-1′′′), 131.44 (C-4′), 130.79 (C-3′′, C-5′′), 128.45 (C-2′′′, C-6′′′), 128.14 (C-4′′), 127.23 (C-2′′, C-6′′), 124.51 (C-2, C-6), 121.97 (C-3′′′, C-5′′′), 114.56 (C-3, C-5), 99.22 (C-2′, C-6′), 74.99 (CH*), 70.80 (**C**H_2OCH*), 68.35 (CH_2O), 56.57 (2 × OCH_3), 31.82 (2 × **C**$H_2CH_2CH_3$), 29.77 (CH_2), 29.40 (**C**$H_2(CH_2)_3O$-b), 29.35 (**C**$H_2(CH_2)_3O$-a), 29.24 (**C**$H_2(CH_2)_2CH_3$), 29.16 (2 × **C**H_2CH_2O), 26.06 (**C**$H_2CH_2CH_2O$-b), 25.99 (**C**$H_2CH_2CH_2O$-a), 22.66 (2 × **C**H_2CH_3), 18.75 (CH***C**H_3), 14.11 (2 × CH_2**C**H_3).

2.2. Mesomorphic properties

The observation of characteristic textures and their changes in polarizing optical microscope (POM) has been carried out on 12 μm thick glass cells, which were filled with LC material in the isotropic phase by means of capillary action. The inner surfaces of the glass plates are covered with Indium-Tin-Oxide (ITO) electrodes and polyimide layers unidirectionally rubbed, which ensures planar alignment of the molecules, e.g. bookshelf geometry in the

smectic phase. A LINKAM LTS E350 heating/cooling stage with TMS 93 temperature programmer was used for the temperature control, which enabled the temperature stabilization within ±0.1 K. Phase transition temperatures and melting points (m.p.) were determined by differential scanning calorimetry (DSC - Pyris Diamond Perkin-Elmer 7) on samples of 5-10 mg, hermetically sealed in aluminium pans, during cooling/heating runs in a nitrogen medium at a heating/cooling rate of 5 K min^{-1}. The temperature was calibrated on the extrapolated onsets of melting points of water, indium and zinc. The enthalpy change was calibrated on the enthalpies of melting water, indium and zinc.

Sequence of phases, phase transition temperatures, melting and clearing points of all investigated materials are shown in Table 1. Depending on the molecular structure, the compounds show quite a different mesomorphic behaviour. The non-chiral **DOBP** compound possesses the nematic (N) and the orthogonal smectic A (SmA) phases over a broad temperature range. The respective characteristic textures for **DOBP** compound are shown in Figure 2. A narrow chiral nematic (cholesteric) phase (N*) has been detected for the chiral **DOLZ** compound. This phase is fully monotropic as it is observed on cooling run only. The chiral **DOTL** compound does not show the liquid crystalline behaviour. The clearing point was detected at substantially low temperatures compare to **DOBP** and **DOLZ** compounds. However, on cooling from isotropic (Iso) phase the material remains liquid down to a very low temperatures; then the glass transition occurs.

[inset Table 1 about here]

[inset Figure 2 about here]

3. Design and characterisation of the photovoltaic cells

Design and basic characteristics of the organic photovoltaic cells doped by functional photo-sensitive materials are described in the following section. The obtained results, namely the UV-Vis spectra, electrochemical measurements, cyclic voltammetry experiments, AFM surface morphology studies and impedance spectroscopy, are presented and discussed.

3.1. Fabrication and characterization of photovoltaic cells

Poly(3-hexylthiophene-2,5-diyl) (P3HT, regioregular) and [6,6]-phenyl C_{61} butyric acid methyl ester (PCBM) were purchased from Sigma-Aldrich and used as received. Poly(3,4-ethylenedioxythiophene):poly(styrene sulfonate) (PEDOT:PSS) was purchased from Ossila company. Methanol, acetone, and chloroform were purchased from POCH Company and used

as received. Special ITO-coated glass substrates were purchased from Ossila Company. Surface resistance of ITO was about 20 Ohm/square.

Solar cells have been fabricated at air atmosphere on an ITO-coated glass substrate, with the structure ITO/PEDOT:PSS/P3HT:PCBM:**X**/Al. The ITO-coated glass substrate was first cleaned with deionised water with further ultra-sonication in isopropanol for about 20 minutes. PEDOT:PSS - was spin cast (1500 turns per minute, 25 sec.) from aqueous solution, to form a film on the ITO substrate. A mixture of P3HT:PCBM:**X** in chloroform solution with a weight ratio 1:0.7:0.09 was then spin cast on top of the PEDOT:PSS layer. An active layer in organic solar cells was not annealed or annealed at various temperatures. The active layer P3HT:PCBM:**X** has been thermally annealed at 55°C for **DOTL** additive, at 108°C, 130°C and 160°C for **DOBP** and at 105°C, 112°C and 128°C for **DOLZ** additive. Then, an aluminium electrode was deposited by thermal evaporation in vacuum of about 5×10^{-5} Torr. Current density–voltage (J–V) characteristics of the devices were measured using a Solar Simulator Model SS100AAA with AM 1.5G. For solar cell performance a xenon lamp with an irradiation intensity of 100 mW/cm^2 was used. The active area of single photovoltaic pixel was about 4.5 mm^2.

UV-Vis spectra have been recorded for chloroform solution and thin films deposited on glass substrate using Jasco V670 spectrophotometer. The solutions were spread on glass using the spin-coating technique.

Electrochemical measurements were carried out using Solartron SI 1287 Electrochemical Interface, ITO electrode, platinum rod and silver wire as working, auxiliary and reference electrode, respectively. Potentials are referenced with respect to ferrocene (Fc), which was used as the internal standard. Cyclic voltammetry experiments were conducted in a standard one-compartment cell, in $CHCl_3$ (POCH, czda grade), under argon. 0.1M Bu_4NPF_6 (Aldrich, 99%) was used as the supporting electrolyte.

The surface morphology studies of the composite mixtures and constructed devices were performed on air using a commercial Innova AFM system from Bruker (former Veeco) company. Measurements were done on air using Tapping Mode along with phase imaging feature. Typical cantilever (about 40 N/m and < 10 nm tip curvature) has been used similarly as in [58].

The final devices were tested with impedance spectroscopy by Solartron precision LCR meter Model SI1260, in the frequency range within 1 Hz - 1 MHz (with test signal value of 20 mV).

In order to study photogeneration of charge carriers in BHJ devices, measurements in dark and under illumination (halogen lamp, 100 mW/cm^2) have been performed.

3.2. Results and discussion

Electrochemical cyclic voltammetry (CV) has been carried out for **DOTL, DOLZ** and **DOBP** solutions on Pt electrode, in order to estimate their HOMO-LUMO energy levels as is presented in Table 2. Moreover we also investigated P3HT and PCBM by CV method. Figure 3a represents the cyclic voltammograms of **DOTL, DOLZ, DOBP** solutions. The HOMO and LUMO energy levels for **DOLZ** are -6.46eV and -3.43eV, respectively. The HOMO levels of **DOTL** and **DOBP**, being quite close to each other, are -5.99eV and -6.05eV, respectively (see Table 2). These values are considerably higher than that for **DOLZ**. The lower value of energy gap (E_g^{CV}) of about 1.90eV has been exhibited by **DOTL**. The **DOLZ** and **DOTL** compounds seem to be promising for testing in ternary active layer in photovoltaic BHJ devices taking into consideration their HOMO-LUMO levels while compare those with HOMO-LUMO levels of P3HT and PCBM (see Figure 3b). The energy diagram of all investigated solar cells is presented in Figure 3.

[Inset Table 2 about here]

[inset Figure 3 about here]

All three **DOTL, DOBP** and **DOLZ** compounds and the respective mixtures with P3HT:PCBM were tested by UV-Vis method in chloroform solution (see Figure 4ab and Table 3). The UV-Vis spectra of all the compounds show two absorption peaks at about 316-339 nm and at about 443-449 nm. Data corresponding to **DOTL** compound exhibits a 23 nm and 4 nm red shift in λ_{1max} in comparison with **DOBP** and **DOLZ** compounds, respectively. All compounds tested as dopants in P3HT:PCBM mixture have no influence on the changes in UV-Vis absorption spectra in chloroform solution (see Table 3). Moreover, in all cases the second UV-Vis absorption band in P3HT:PCBM:**X** thin film spectrum (X stands for **DOTL, DOBP** and **DOLZ** compounds while doping) at ambient temperature was about 9-13 nm blue-shifted in comparison with the P3HT:PCBM layer without organic dopants (**X**) (see Table 3).

[inset Figure 4 about here]

[inset Table 3 about here]

It is worth mentioning that the UV-Vis absorption second band of P3HT:PCBM:**X** thin film spectrum, measured at ambient temperature, was about 29-33 nm red shifted in comparison

with that detected in chloroform solution. The obtained data confirms that the molecule conformations or aggregation tendencies measured in solution and in film are quite different.

The bulk heterojunction (BHJ) organic solar cells were fabricated with a structure ITO/PEDOT:PSS/P3HT:PCBM:**X**/Al, where **X** stands for **DOTL, DOBP** and **DOLZ** compounds used as functional dopants. The current density–voltage (J–V) curves of the selected polymeric photovoltaic devices measured under AM1.5G-simulated solar illumination of 100 mW/cm^2 are shown in Figure 5. The resulting characteristics of OPVs are summarized in Table 4.

[inset Figure 5 about here]

[inset Table 4 about here]

The revealed results demonstrate an additive influence of the chemical structure of the functional organic dopants and applied annealing process on the photovoltaic (PV) properties. Our study showed that the photovoltaic properties of the constructed polymer solar cells doped with organic compounds are strongly affected by the chemical structure of the organic compound and annealing (see Table 3). Two compounds (**DOBP** and **DOLZ**) possessing the self-assembling behaviour (i.e. liquid crystallinity) and one compound with a direct phase transition from the isotropic to crystals state (**DOTL**) have been used as functional dopants. Taking into consideration the influence of the chemical structure of the used organic compounds on the PV performances of the constructed polymer solar cells, it becomes obvious that the best performance has been obtained at RT for the device doped with **DOLZ** (see Table 4 and Fig. 5). It is worth to mention that the device doped with **DOBP** exhibited the lowest value of PCE in comparison with other dopants used in this work. Chemical structure of **DOBP** and **DOLZ** compound are quite similar. However, in P3HT:PCBM active layer they are working in a different way and consequently the PCE value for **DOBP** substantially decreases (for about three times) compare to that of **DOLZ** (see Table 4). Such a behaviour can be explained by different aliphatic chain lengths, namely $OC_{12}H_{13}$ and OC_8H_{13}, in **DOBP** in comparison with that of **DOTL** and **DOLZ** compounds. Consequently **DOTL** compound, possessing one phenyl ring less than **DOBP** and two aliphatic chains with similar length (OC_6H_{13} and OC_8H_{13}), exhibited more than two times higher value of PCE than the device with **DOBP** dopant (see Table 4).

The chemical structure of the compounds used as dopants has a strong effect on the value of short circuit current density (J_{sc}) (see Table 4), which increases from 1.16 mA/cm^2 to 2.23 mA/cm^2 for devices doped with **DOBP** and **DOLZ**, respectively. On other hand, there is no

significant effect of the dopant in P3HT:PCBM active layer on the open circuit voltage (V_{oc}) and fill factor (FF).

In order to investigate the origin of increase J_{sc} and PCE morphologies of active layers with various organic compounds, AFM studies have been done and are presented in Fig. 6.

[inset Figure 6 about here]

The value of root mean roughness parameter (S_q) [70] was found to be the highest for P3HT:PCBM:**DOTL**, while for active layer with **DOLZ** S_q parameter was found to be the lowest among thee investigated samples. The possible reason of such a difference might be quite different distribution of dopants in the P3HT:PCBM active layer (see Fig. 6). For the case of P3HT:PCBM:**DOTL** sample, probably **DOTL** molecules are mainly located on the P3HT:PCBM layer, causing the increase of S_q parameter. A quite low value of S_q parameter in the case of P3HT:PCBM:**DOLZ** indicates that probably all the **DOLZ** molecules are located within the P3HT:PCBM active layer. The case of P3HT:PCBM:**DOBP** layer is a intermediate one (with respect to the described above cases); as a result the S_q roughness is higher than that for **DOLZ** but lower than for **DOTL** dopants.

The P3HT:PCBM:**DOTL** sample is covered with hemispherical objects with diameter within 300 - 3000 nm, and 10 - nm height. The surface coverage ratio with described objects is about 40%. The morphology of P3HT:PCBM:**DOBP** sample is much more complex as it reveals the presence of hemispherical objects of 250 – 450 nm diameter and 6 – 30 nm height, covered by the grainy, approx. 10 nm in diameter, film. Furthermore, one can notice the presence of flat, linear features creating regular, step-like structures on that film that reveals a structural ordering. The single layer thickness of such an object is approximately 2.5 nm and it is multiplied in case of thicker ones. The thickness of observed objects varies within 2.5 - 30 nm range. The length and width of those structures varies within 400 - 6000 nm and 40 - 300 nm, respectively. It can be noticed that some of the features are less regular and reveal the corrugation of the sample. The surface of P3HT:PCBM:**DOLZ** contains hemispherical objects of 100 – 300 nm diameter and 5 -20 nm height, covered by a film made of the network of fibres (10 nm radius). The film is covered by two kinds of the regularly formed features. The features of the first kind are placed over the surface with 85% coverage ratio, and the shapes of those features are irregular. Unlike the features of the first kind, the second ones create distinct, regular and relatively flat objects. It has to be underlined that the lateral size of those features are smaller than in the case of P3HT:PCBM:**DOBP**, and vary within 400 - 4000 nm and 100 – 300 nm for length and width, respectively. No preferential orientation of the features has been detected.

The constructed BHJ polymer solar cells doped by specific organic compounds in active layer have been investigated also by impedance spectroscopy (EIS). Nyquist plots for all the devices with non-annealed active layer are presented in Fig. 7 along with an equivalent circuit of ITO/PEDOT:PSS/P3HT:PCBM:**X**/Al devices. R_S represents the series resistance, C_G is the capacitance between anode and cathode, R is resistance and $Q=1/(T\cdot(j\cdot\omega)^p)$ is a constant phase element of the investigated layer, where T and $|p|\leq 1$ are the parameters. When $0<p<1$ then the parameters correspond to some distribution of charge transport processes rather than to a single one. Recently, impedance spectroscopy of OPV devices with P3HT:PCBM active layer has been reported [71].

[inset Figure 7 about here]

All studied devices a with non-annealed active layer exhibit semicircles in Nyquist plots. Two semicircles can be easily distinguished in the case of ITO/PEDOT:PSS/P3HT:PCBM: **DOBP**/Al (see Fig. 7). Moreover, an evident effect on values of the real part (Z') and the imaginary part (Z") of complex impedance along with a change of the chemical structure of the additive can be observed that results in a decrease of semicircles diameter (see Fig. 7). The diameter of the semicircle for the BHJ solar cell doped with **DOTL** compound is the largest while device doped with **DOLZ** compound exhibits the smallest semicircle diameter. This reflects a creation of additional charge carriers under device illumination along with using of various dopants.

The mean relaxation times $\tau_m = (RT)^{1/p}$ (where T: Q-T and p: Q-P) have been calculated (see Table 5). The lowest values of mean relaxation time have been reached for **DOLZ** doped device (with a non-annealed active layer) because a consequence of the charge carrier generation by incident photons in the **DOLZ** doped active layer leads to larger concentration of free carriers.

[inset Table 5 about here]

The effect of temperature on the PV parameters of constructed polymer solar cells has been investigated. (see Table 4). The best performance was found for devices with P3HT:PCBM:**X** non-annealed active layers which is opposite to our previous results of doping by two compounds possessing the self-assembling properties [57]. Unambiguously the device with P3HT:PCBM:**DOLZ** active layer (annealed at 105°C and 128°C) has showed about two times lower PCE value than that of the non-annealed device. Moreover, this device with active layer annealed at 112°C exhibited ten times lower value than that with the non-annealed one. For **DOBP** compound the highest value of PCE was found for the devices with a non-annealed

active layer and for active layer annealed at 160°C (see Table 4). Although, a very poor PV effect has been observed for **DOBP** doped devices with active layers annealed at 108°C and 130°C. On the other hand, independently on the annealing temperature the same value of PCE has been found for **DOTL** (without self-assembling behaviour) doped solar cells (see Table 4). Devices with a non-annealed active layer exhibit the highest charge transport properties. Consequently, a poor performance of the device with annealed active layer can be attributed to the morphology change of active layer which probably results in an unbalanced charge extraction leading to the observed characteristics.

The values of short circuit current density (J_{sc}) for the devices with the annealed P3HT:PCBM:**DOLZ** active layer are slightly lower than that for the non-annealed device (see Table 4 and Fig. 5). Similar behaviour has been observed for **DOBP** doped active layer annealed from 108°C to 130°C.

It is quite exciting that for P3HT:PCBM:**DOBP** device with annealed active layer at 160°C value of J_{sc} equals 1.43 mA/cm^2 was about 0.27 mA/cm^2 higher than that for the device with the non-annealed active layer (1.16 mA/cm^2); consequently value of PCE is almost identical for devices with non-annealed and annealed active layers (see Table 4). Similar behaviour has been found for the device with P3HT:PCBM:**DOTL** active layer annealed at 55°C. In this case J_{sc} value has been found ~0.34 mA/cm^2 higher than that for the device with a non-annealed active layer (see Table 4).

Short circuit current density (J_{sc}) strongly depends on the efficiencies of the light absorption of the active layer and on broadness and maximum of the absorption band. To further investigate, UV-Vis absorption spectra of P3HT:PCBM:**X** films have been tested before and after thermal annealing (see Fig. 8 and Table 2). In UV-Vis spectra of the P3HT:PCBM:**X** films red shift of the second absorption band with the temperature increase has been observed (Table 2). Moreover, along with the temperature increase, third absorption band (shoulder) appears at about 600 nm (see Table 2 and Fig. 8).

[inset Figure 8 about here]

The second absorption band of P3HT:PCBM:**DOTL** film (about 480 nm at RT) was about 24 nm batochromically shifted along with the temperature increase to 55 °C. For P3HT:PCBM:**DOBP** film along with the temperature increase from RT to 160 °C the second absorption band was 18 nm red shifted. While for P3HT:PCBM:**DOLZ** film along with the temperature increase from RT to 128 °C the second absorption band was 22 nm red shifted.

The changes of absorption spectra along with the temperature increase can be explained by the geometric isomers (*E* and *Z*) and by aggregation of the organic compounds within this temperature range, which is induced by the isomerisation in the ground state as proposed by Ogawa et al. [72-73]. If the azo group is present, two isomers (*E* and *Z*) can exist at some ratio, even though the *E* structure is always supposed to be thermodynamically more stable. Similar behaviour has been found for the salicylideneanilines and polyazomethines [74-75]. The changes of the absorption properties of the imine under temperature change confirmed the conformational changes in the conjugating backbone structure of the compound. However, for azo compounds, only *Z-E* isomerisation is operating thermally in the ground state so the actual aggregation can be triggered by something else. If it was triggered by isomerisation, it would also take place during illumination by xenon lamp, because of the *E/Z* photoisomerisation. We are able to confirm the *E/Z* photoisomerisation of used dopants from the substantial changes in UV-Vis absorption spectra only in solution. However, it was not possible to confirm the *E/Z* photoisomerisation of a dopant (in the active layer) in solid state, since the spectral changes upon illumination are negligible.

In order to check if the investigated organic dopants have an influence on the lifetime of constructed polymer solar cells, all devices were tested again after 10 months (encapsulated devices were kept in laboratory in the air atmosphere). The lowest losses in PCE (about 57%) have been found for device with P3HT:PCBM:**DOLZ** active layer annealed at 112 °C (see Table 4). For the device without organic dopant in P3HT:PCBM active layer PCE losses were about 30% after 10 months. For device with P3HT:PCBM:**DOBP** active layer annealed at 108°C PCE losses were about 70% after 10 months. It is quite unexpected and exciting that investigated polymer solar cells doped with LC compounds exhibited better values of PCE for non-annealed than annealed active layer. However in some cases annealing of active layer affects positively the lifetime of devices (see Table 5), i.e. the lifetime of the devices increases while doping. This part of our work needs more investigations which are in progress now and will be presented separately elsewhere.

To make the situation more clear, the morphology of P3HT:PCBM:**X** active layer annealed at selected temperatures has been studied by AFM (see Fig. 9). While compare the annealed and non-annealed active layers definite differences in formation of aggregates morphologies can be clearly observed. For P3HT:PCBM:**DOTL** active layer (annealed at 55°C) values of S_q were found to be the lowest compare to that for non-annealed active layer (compare Figs. 6 and 9). Similar behaviour has been found for P3HT:PCBM:**DOLZ** active layer annealed at

128°C. An opposite behaviour has been found only for P3HT:PCBM:**DOBP** active layer annealed at 160 °C (see Figs. 6 and 9).

[inset Figure 9 about here]

The AFM-based morphological analysis of developed samples revealed a minor effect of P3HT:PCBM:**DOTL** surface annealing. However, the presence of hemispheres of abovementioned size can be still detected. In the case of P3HT:PCBM:**DOBP** active layer, the substantial morphology changes are found. The density of hemispherical objects decreases and the dimensions (specifically the width) of the features increase. It can be assumed that the features agglomerated during annealing, while the lower layers of the sample flattened. The P3HT:PCBM:**DOLZ** sample morphology was changed in a distinct manner. Abovementioned agglomeration of the features is more apparent than in case of P3HT:PCBM:**DOBP**, as in general only two fractions (the film and the flat features) are present. Although the thickness of the features did not change (2 nm remained), their lateral dimensions increased significantly, as they have been transformed into irregular shape island-like objects, covering the surface with 45% ratio. No privileged orientation of the edges of the features has been observed.

All studied devices with an active layer annealed at various temperatures exhibit semicircles in Nyquist plots (see Fig. 10). For the **DOLZ** and **DOTL** doped devices an evident drop in values of the real part (Z') and the imaginary part (Z") of complex impedance, along with increase temperature of active layer annealing, has been observed. This reflects a creation of additional charge carriers under device illumination.

[inset Figure 10 about here]

The mean relaxation time of investigated devices was changed in all the considered cases along with temperature increase under illumination (see Table 5). This part of our work requires more detailed investigations, which are in progress now and will be presented elsewhere.

4. Conclusion

Three new organic compounds designed with a specific molecular structure (with and without a self-assembling behaviour) have been synthesised and characterised. The non-chiral **DOBP** compound possesses the nematic and the orthogonal smectic A phases over a broad temperature range. A narrow chiral nematic (cholesteric) phase has been detected for the chiral **DOLZ** compound. This phase is fully monotropic as it is observed on cooling run only. The chiral **DOTL** compound does not show the liquid crystalline behaviour. These materials

were used as a functional dopants for P3HT:PCBM active layer of in order to establish the effect of doping on the BHJ solar cells properties and characteristics. From the electrochemical and optical analysis the HOMO-LUMO and absorption properties have been detected. The HOMO energy level for **DOLZ, DOTL** and **DOBP** are -6.46eV, -5.99eV and -6.05eV, respectively. The UV-Vis spectra of all the compounds in chloroform solution show two absorption peaks at about 316-339 nm and at about 443-449 nm. All compounds tested as dopants in P3HT:PCBM mixture have no influence on the changes in UV-Vis absorption spectra. The highest power conversion efficiency, which was equal to 0.34 % under simulated 100 mW/cm^2 AM 1.5G irradiation, was determined for the device using **DOLZ** with the ITO/PEDOT: PSS/P3HT:PCBM:**DOLZ**/Al architecture. A chemical structure of the compounds used as dopant has a strong effect on the value of short circuit current density (J_{sc}) which increases from 1.16 mA/cm^2 to 2.23 mA/cm^2 for devices doped with **DOBP** and **DOLZ**, respectively. There is no significant effect of the dopant in P3HT:PCBM active layer on the open circuit voltage (V_{oc}) and fill factor (FF). BHJ polymer solar cells with ITO/PEDOT:PSS/P3HT:PCBM:**X**/Al architecture were constructed and analysed by J-V characteristics and EIS spectroscopy taking into consideration (i) the specific chemical structure of the compounds used as functional dopants and (ii) the annealing temperature of active layer. It has been shown that the P3HT:PCBM:**DOLZ** device with non-annealed active layer possesses the best behaviour with respect to other considered structures and has a good chance to be used as a prototype for the commercial photovoltaic cells production. Further studies are in progress now and the results will be presented elsewhere.

Acknowledgements

Authors are greatly acknowledging the financial support from the research projects: COST IC1208, MEYS LD14007, CSF 16-12150S and MEYS LH15305. The authors greatly acknowledge the bilateral Polish-Czech project No 7AMB13PL038 funded by Ministry of Science and Higher Education (Poland) and Ministry of Education, Youth and Sports (Czech Republic).

References

[1] H. Dong, H. Zhu, Q. Meng, X. Gong, W.Hu, *Chem. Soc. Rev.*, 2012, **41**, 1754.

[2] H. Němec, E. Galoppini, H. Imahori, V. Sundstrom, *Comprehensive Nanoscience and Technology,* 2011, **2**, 325.

[3] J. Burschka, N. Pellet, S.-J. Moon, R. Humphry-Baker, P. Gao, M. K. Nazeeruddin, M. Grätzel, *Nature,* 2013, **499**, 316.

[4] M. Liu, M. B. Johnston, H. J. Snaith, *Nature,* 2013, **501**, 395.

[5] H. Zhou, Q. Chen, G. Li, S. Luo, T.-B. Song, H.-S. Duan, Z. Hong, J. You, Y. Liu, Y. Yang, *Science,* 2014, **345**, 542.

[6] G. Yu, J. Gao, J. C. Hummelen, F. Wudl, A. J. Heeger, *Science,* 1995, **270**, 1789.

[7] K. Sun, Z. Xiao, S. Lu, W. Zajaczkowski, W. Pisula, E. Hanssen, J. M. White, R.M. Williamson, J. Subbiah, J. Ouyang, A. B. Holmes, W. W. H. Wong, D. J. Jones, *Nature Communications,* 2015, **6**, 6013.

[8] G. Li, R. Zhu, Y. Yang, *Nature Photonics,* 2012, **6**, 153.

[9] K. D. G. I. Jayawardena, L. J. Rozanski, C. A. Mills, M. J. Beliatis, N. A. Nismy, S. R. P. Silva, *Nanoscale,* 2013, **5**, 8411.

[10] W. Cai, X. Gong, Y. Cao, *Sol. Energ. Mat. Sol. C,* 2010, **94**, 114.

[11] Y. Li, *Acc. Chem. Res.,* 2012, **45**, 723.

[12] H. Zhou, L. Yang, W. You, *Macromolecules,* 2012, **45**, 607.

[13] Jian-Sheng Li, Xiao-Jing Sang, Wei-Lin Chen, Rong-Lin Zhong, Ying Lu, Lan-Cui Zhang, Zhong-Min Su and En-Bo Wang, *RSC Advances*, 2015, **5**, 8194.

[14] K.Yuan, L. Chen, Y. Chen, *J. Mater. Chem. C*, 2014, **2**, 3835.

[15] G. Li, R. Zhu, Y. Yang, *Nature Photonics,* 2012, **6**, 153.

[16] W. Chen, Y. Chen, F. Li, L. Chen, K. Yuan, K. Yao, P. Wang, *Sol. Energ. Mat. Sol. C,* 2012, **96**, 266.

[17] M. Palewicz, A. Iwan, M. Sibiński, A. Sikora, B. Mazurek, *Energy Procedia,* 2011, **3**, 84.

[18] K. Yao, L. Chen, T. Hua, Y. Chen, *Org. Electron.,* 2012, **13**, 1443.

[19] S. A. Myers, M. S. Al Kalifah, C. Lei, M. O'Neill, S.P.Kitney, S. M. Kelly, *Sol. Energ. Mat. Sol. C,* 2013, **116**, 262.

[20] L. Wang, S-Y. Park, S-M. Kim, S. Yoon, S-H. Lee, E. Lee, K-U. Jeong, M-H. Lee, *Liquid Crystals,* 2012, **39**, 795.

[21] L. Li, S-W. Kang, J. Harden, Q. Sun, X. Zhou, L. Dai, A. Jakli, S. Kumarb, Q. Li, *Liquid Crystals,* 2008, **35**, 233.

[22] T. Nhu, Y Hoang, D. Pociecha, M. Salamonczyk, E. Gorecka, R. Deschenaux, *Soft Matter,* 2011, **7**, 4948.

[23] Q. Zheng, G. Fang, W. Bai, N. Sun, P. Qin, X. Fan, F. Cheng, L. Yuan, X. Zhao, *Sol. Energ. Mat. Sol. C,* 2011, **95**, 2200.

[24] S. Jeong, Y. Kwon, B-D. Choi, H. Ade, Y. S. Han, *Appl. Phys. Lett.,* 2010, **96**, 183305.

[25] N. Y. Canli, S. Gunes, A. Pivrikas, A. Fuchsbauer, D. Sinwel, N. SSariciftci, O. Yasa, B. Bilgin-Eran, *Sol. Energ. Mat. Sol. C*, 2010, **94**, 1089.

[26] A. Iwan, M. Palewicz, M. Krompiec, M. Grucela-Zajac, E. Schab-Balcerzak, A. Sikora, *Spectrochim. Acta Part A: Molec. Biomolec. Spectr.*, 2012, **97**, 546.

[27] F. Lincker, B. Heinrich, R. De Bettignies, P. Rannou, J. Pecaut, B. Grevin, A. Pron, B. Donnio, R. Demadrille, J. Mater. Chem., 2011, **21**, 5238.

[28] H.-K. Kwon, K.-T. Lee, K. Hur, S. H. Moon, M. M. Quasim, T. D. Wilkinson, J.-Y. Han, H. Ko, I.-K. Han, B. Park, B. K. Min, B.-K. Ju, S. M. Morris, R. H. Friend, D.-H. Ko, *Advanced Energy Materials,* 2015, **5**(3), doi: 10.1002/aenm.201401347.

[29] M. Carrasco-Orozco, W. C. Tsoi, M. O'Neill, M. P. Aldred, P. Vlachos, S. M. Kelly, *Advanced Materials,* 2006, **18**, 1754.

[30] K.-H. Kim, H. Yu, H. Kang, D.J. Kang, C-H. Cho, H-H. Cho, J.H. Oh, B.J. Kim, *J. Mater. Chem. A*, 2013, **1**, 14538.

[31] P. A. Troshin, D. K. Susarova, E. A. Khakina, A. A. Goryachev, O. V. Borshchev, S. A. Ponomarenko, V. F. Razumov, N. S. Sariciftci, *J. Mater. Chem.*, 2012, **22**, 18433.

[32] B. H. Wunsch, M. Rumi, N. R. Tummala, C. Risko, D.-Y. Kang, K. X. Steirer, J. Gantz, M. Said, N. R. Armstrong, J.-L. Bredas, D. Bucknall, S. R. Marder, *J. Mater. Chem. C*, 2013, **1**, 5250.

[33] D. J. Broer, J. A. M. M. van Haaren, C. W. M. Bastiaansen, *e-Polymers*, 2001, 023.

[34] J. P. F. Lagerwall, G. Scalia, *Current Appl. Phys.*, 2012, **12**, 1387.

[35] J. P. F. Lagerwall, F. Giesselmann, *Chem Phys Chem*, 2006, **7**, 20.

[36] O. Stamatoiu, A. Bubnov, I. Tarcomnicu, M. Iovu, *J. Mol. Struct.*, 2008, **886**, 187.

[37] A. Bubnov, V. Novotná, V. Hamplová, M. Kašpar, M. Glogarová, *J. Mol. Struct.*, 2008, **892**, 151.

[38] V. Domenici, J. Milavec, A. Bubnov, D. Pociecha, B. Zupančič, A. Rešetič, V. Hamplová, E. Gorecka, B. Zalar, *RSC Advances*, 2014, **4**, 44056.

[39] J. Milavec, V. Domenici, B. Zupancic, A. Rešetič, A. Bubnov, B. Zalar, *Phys. Chem. Chem. Phys.,* 2016, doi: 0.10016/j.jphoto%20chem.2015.10.021.

[40] A. Bobrovsky, V. Shibaev, A. Bubnov, V. Hamplová, M. Kašpar, M. Glogarová, *Macromolecules*, 2013, **46**, 4276.

[41] A. Bubnov, V. Novotná, V. Hamplová, M. Kašpar, M. Glogarová, *Phase Transitions* 2012, **85**, 849.

[42] D. Ž. Obadović, A. Vajda, M. Garić, A. Bubnov, V. Hamplová, M. Kašpar, K. Fodor-Csorba, *J. Therm. Anal. Calorim.*, 2005, **82**, 519.

[43] A. Pramanik, B. Das, M. K. Das, V. Hamplová, M. Kašpar, A. Bubnov, *Phase Transitions*, 2015, **88**, 745.

[44] A. Bubnov, V. Hamplová, M. Kašpar, A. Vajda, M. Stojanović, D.Ž. Obadović, N. Éber, K. Fodor-Csorba, *J. Therm. Anal. Calorim.*, 2007, **90**, 431.

[45] A. Bubnov, V. Hamplová, M. Kašpar, P. Vaněk, D. Pociecha, M. Glogarová, *Molecular Crystals and Liquid Crystals Science and Technology Section A: Molecular Crystals and Liquid Crystals*, 2001, **366**, 547.

[46] A. Bubnov, M. Kašpar, V. Hamplová, U. Dawin, F. Giesselmann, *Beilstein Journal of Organic Chemistry,* 2013, **9**, 425.

[47] A. Bobrovsky, V. Shibaev, M. Cigl, V. Hamplova, F. Hampl, G. Elyashevitch, *Journal of Materials Chemistry C*, 2014, **2**, 4482.

[48] A. Bobrovsky, V. Shibaev, A. Bubnov, V. Hamplová, M. Kašpar, D. Pociecha, M. Glogarová, *Macromol. Chem. Phys.*, 2011, **212**, 342.

[49] T. Tóth-Katona, M. Cigl, K. Fodor-Csorba, V. Hamplová, I. Jánossy, M. Kašpar, T. Vojtylová, F. Hampl, A. Bubnov, *Macromol. Chem. Phys.*, 2014, **215**, 742.

[50] A. Bobrovsky, V. Shibaev, G. Elyashevitch, E. Rosova, A. Shimkin, V. Shirinyan, A. Bubnov, M. Kašpar, V. Hamplová, M. Glogarová, *Liquid Crystals*, 2008, **35**, 533.

[51] M. Kašpar, A. Bubnov, Z. Sedláková, M. Stojanović, J. Havlíček, D. Ž. Obadović, M. Ilavsky, *European Polymer Journal*, 2008, **44**, 233.

[52] A. Bubnov, V. Domenici, V. Hamplová, M. Kašpar, B. Zalar, *Polymer*, 2011, **52**, 4490.

[53] A. Bubnov, M. Kašpar, V. Hamplová, M. Glogarová, S. Samaritani, G. Galli, G. Andersson, L. Komitov, *Liquid Crystals*, 2006, **33**, 559.

[54] S.K. Nisha, S.K. Asha, *J. Mat. Chem. C*, 2014, **2**, 2051.

[55] S. Saliba, Ch. Mingotaud, M. L. Kahn, J.-D. Marty, *Nanoscale*, 2013, **5**, 6641.

[56] M. Stojanović, A. Bubnov, D.Ž. Obadović, V. Hamplová, M. Cvetinov, M. Kašpar, *Mat. Chem. Phys.*, 2014, **146**, 18.

[57] A. Iwan, B. Boharewicz, I. Tazbir, V. Hamplová, A. Bubnov, *Solid State Electronics*, 2015, **104**, 53.

[58] A. Iwan, A. Sikora, V. Hamplová, A. Bubnov, *Liquid Crystals,* 2015, **42**, 964.

[59] M. Kašpar, A. Bubnov, V. Hamplová, S. Pirkl, M. Glogarová, *Liquid Crystals*, 2004, **31**, 821.

[60] V. Novotná, V. Hamplová, A. Bubnov, M. Kašpar, M. Glogarová, N. Kapernaum, S. Bezner, F. Giesselmann, *J. Mater. Chem.*, 2009, **19**, 3992.

[61] A. Bobrovsky, V. Shibaev, V. Hamplová, A. Bubnov, V. Novotná, M. Kašpar, A. Piryazev, D. Anokhin, D. Ivanov, *J. Photochem. Photobiol. A: Chem.,* 2016, **316**, 75.

[62] P. Perkowski, A. Bubnov, M. Mrukiewicz, D. Pociecha, W. Piecek, V. Hamplová, M. Kašpar, *Phase Transitions*, 2014, **87**, 1024.

[63] W. Piecek, A. Bubnov, P. Perkowski, P. Morawiak, K. Ogrodnik, W. Rejmer, M. Zurowska, V. Hamplová, M. Kašpar, *Phase Transitions*, 2010, **83**, 551.

[64] A. Bubnov, M. Tykarska, V. Hamplová, K. Kurp, *Phase Transitions*, 2015, doi: 10.1080/01411594.2015.1087523

[65] Ravi K. Shukla, K. K. Raina, V. Hamplová, M. Kašpar, A. Bubnov, *Phase Transitions*, 2011, **84**, 850.

[66] V. Novotná, J. Vejpravová, V. Hamplová, J. Prokleška, E. Gorecka, D. Pociecha, N. Podoliak, M. Glogarová, *RSC Advances*, 2013, **3**, 10919.

[67] A. Iwan*, Renewable and Sustainable Energy Reviews,* 2015, **52**, 65.

[68] W. S. Johnson, C. D. Gutsche, R. D. Offenhauer, *J. Am. Chem. Soc.,* 1946, **68**, 1648.

[69] S. Kobayashi, S. Ishibashi, *Mol. Cryst. Liq. Cryst.,* 1992, **220**, 1.

[70] http://www.imagemet.com/WebHelp6/Default.htm#RoughnessParameters/Roughness_Parameters.htm

[71] A. Iwan, M. Palewicz, M. Ozimek, A. Chuchmala, G. Pasciak, *Org. Electr.,* 2012, **13**, 2525.

[72] K. Ogawa, J. Harada, T. Fujiwara, S. Yoshida, *J. Phys. Chem. A,* 2001, **105**, 3425,

[73] A. Ohshima, A. Momotake, T. Arai, *J. Photochem. Photobiol. A: Chem.,* 2004, **162**, 473.

[74] A. Iwan, D. Sek, *Progress Polym. Sci.,* 2008, **33**, 289.

[75] D. Tsang, M. Bourgeaux, W. G. Skene, *J. Photochem. Photobiol. A: Chem.,* 2007, **192**, 122.

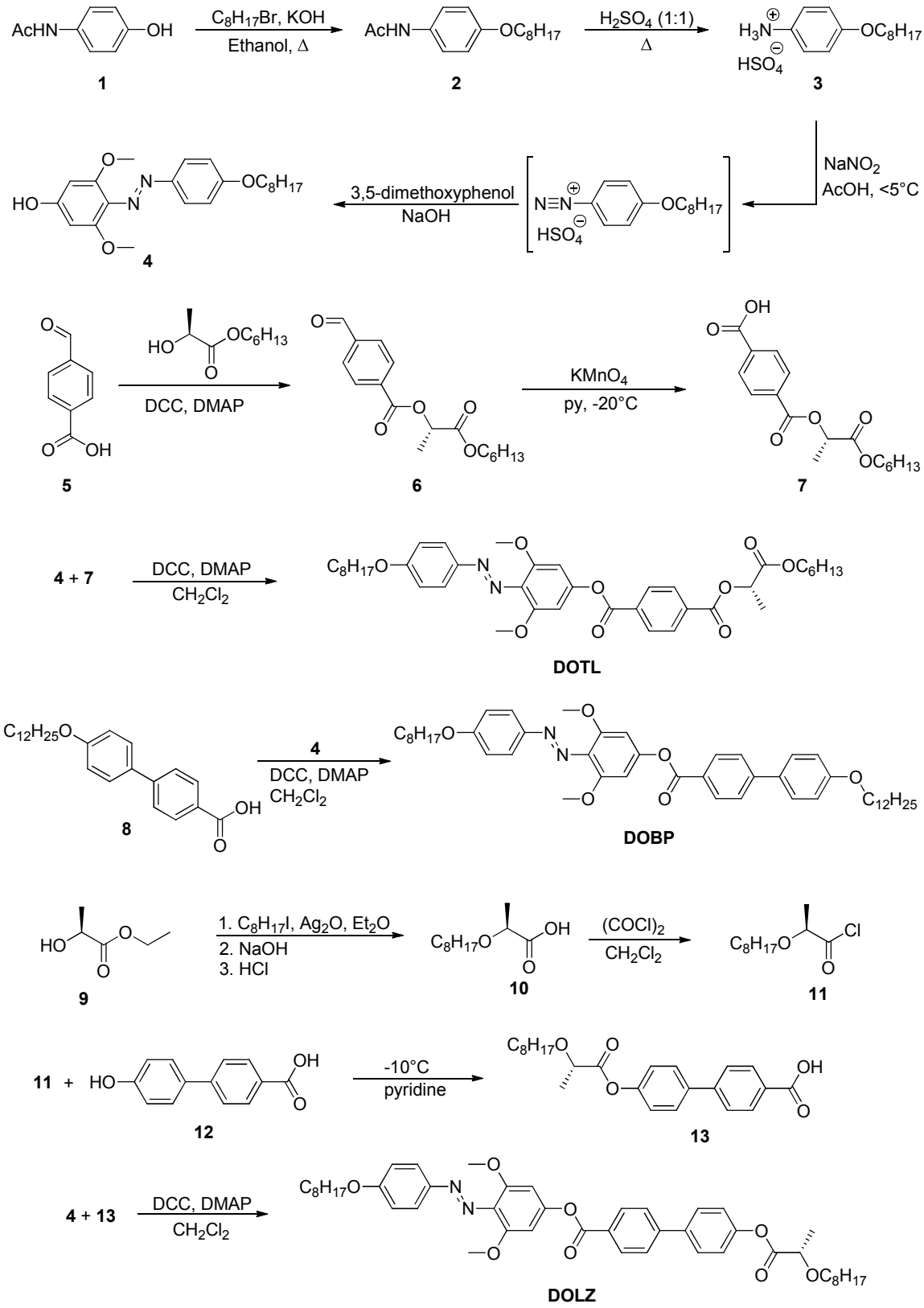

Figure 1. General procedure for the synthesis of new photosensitive compounds.

Table 1. Sequence of phases, phase transition temperatures (^{o}C) and phase transition enthalpies [ΔH] (KJ/g) of the investigated compound obtained on cooling (5 Kmin^{-1}); from the isotropic phase; melting point, m.p., and clearing point, c.p., obtained on heating (5 Kmin^{-1}) for newly synthesised compounds.

Compound	m.p.	c.p.	phase	T[°C]	phase	T[°C]	phase	T[°C]	phase
DOBP	128.4	157.7	Cr	107.3	**SmA**	135.4	**N**	156.8	**Iso**
(non-chiral)	[+59.2]	[+1.5]		[-29.9]		[-0.9]		[-1.6]	
DOLZ	128.0	128.0	Cr	103.1	-		**N***	112.3	**Iso**
(chiral)	[+46.6]	[+46.6]		[-38.4]				[-1.3]	
DOTL	54.8	54.8	Tg	-16.3	-		-		**Iso**
(chiral)	[+52.0]	[+52.0]		[0.447]					

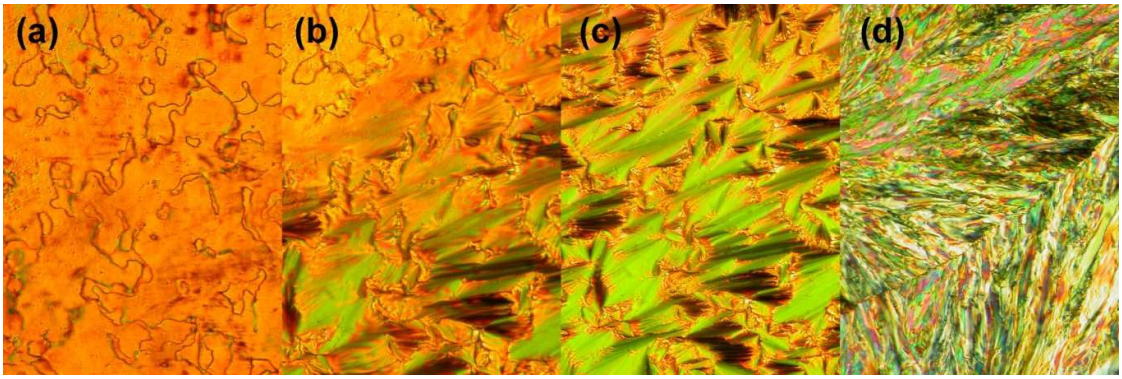

Figure 2. Microphotographs of the mesophase textures obtained by POM for **DOBP** compound (the same area of the cell): (a) nematic schlieren texture at 150^{o}C, (b) phase transition from the nematic to the SmA phase at about 135^{o}C, (c) fan-shaped texture of the SmA phase at 130^{o}C, (d) crystal phase texture at 100^{o}C. Width of the microphotographs is about 250 μm.

Table 2. Electrochemical properties of **DOTL**, **DOLZ** and **DOBP** dopants, P3HT and PCBM materials determined in solution. HOMO and LUMO energy levels are indicated.

Code	E^{ox}_{onset} [V]	E^{red}_{onset} [V]	E_g^{CV} [eV]	HOMO [eV]	LUMO [eV]
DOTL	1.19	-0.72	1.90	-5.99	-4.08
DOLZ	1.66	-1.37	3.03	-6.46	-3.43
DOBP	1.25	-2.11	3.36	-6.05	-2.69
P3HT	0.73	-1.15	1.88	-5.13	-3.25
PCBM	1.56	-0.58	2.13	-5.96	-3.82

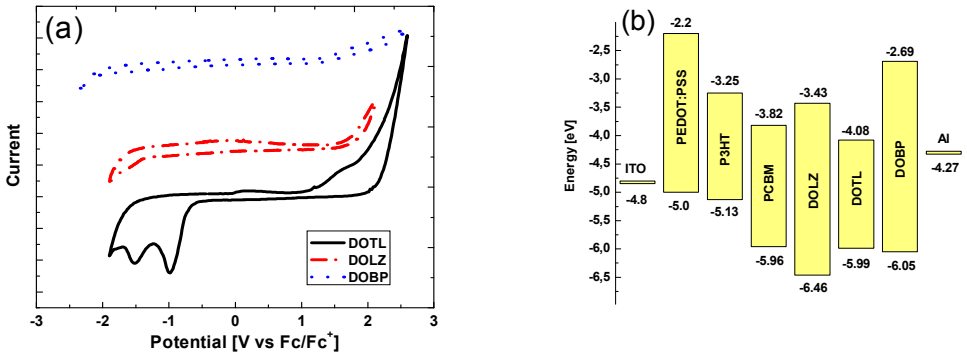

Figure 3. Cyclic voltammograms of 0.2 mM for **DOTL, DOLZ,** and **DOBP** compounds (a). Supporting electrolyte: 0.1 M Bu_4NPF_6 /chloroform under Ar. Potential limits: -2.5/+2.5 V scan rate: 100 mV/s. The energy level diagram of donor and acceptors based on CV experiment and the work function of the different electrodes (b).

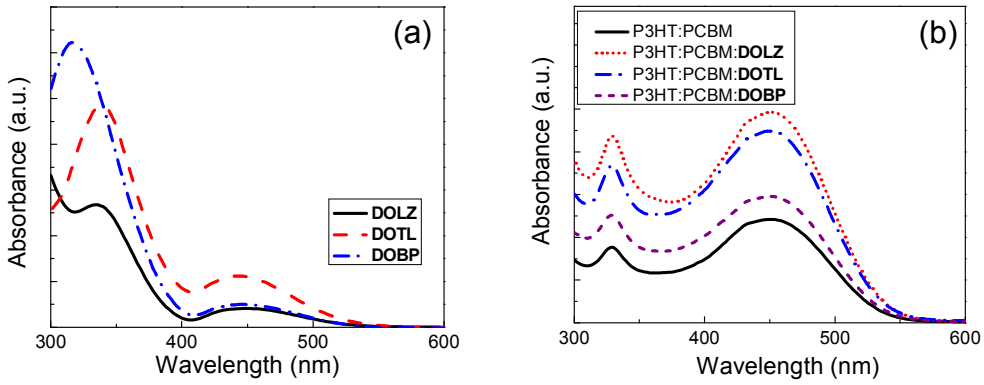

Figure 4. UV-Vis absorption spectra of pure **DOTL, DOBP** and **DOLZ** compounds (a) and P3HT:PCBM:**X** mixtures (b) in chloroform solution (where **X** stands for the one of the doped compound as indicated).

Table 3. Comparison of absorption properties (λ_{1max}, λ_{2max}, λ_{1max} in nm) for investigated compounds and resulting mixtures in chloroform solution and in films at indicated temperatures. An abbreviation RT stands for room temperature.

In $CHCl_3$ solution	**UV-Vis**		
	λ_{1max}	λ_{2max}	λ_{3max}
DOTL (RT)	339	443	-
DOBP (RT)	316	447	-
DOLZ (RT)	335	449	-
P3HT:PCBM:**DOTL** (RT)	329	451	-
P3HT:PCBM:**DOBP** (RT)	329	451	-
P3HT:PCBM:**DOLZ** (RT)	329	451	-
P3HT:PCBM (RT)	329	451	-
In film			
P3HT:PCBM:**DOTL** (RT)	334	480	-
P3HT:PCBM:**DOTL** (55°C)	334	504	-
P3HT:PCBM:**DOBP** (RT)	334	482	-
P3HT:PCBM:**DOBP** (108°C)	334	502	600
P3HT:PCBM:**DOBP** (130°C)	334	486	607
P3HT:PCBM:**DOBP** (160°C)	334	500	600
P3HT:PCBM:**DOLZ** (RT)	334	484	-
P3HT:PCBM:**DOLZ** (105°C)	334	502	600
P3HT:PCBM:**DOLZ** (112°C)	334	504	600
P3HT:PCBM:**DOLZ** (128°C)	334	506	600
P3HT:PCBM (RT)	334	493	-
P3HT:PCBM (130°C)	334	498	603

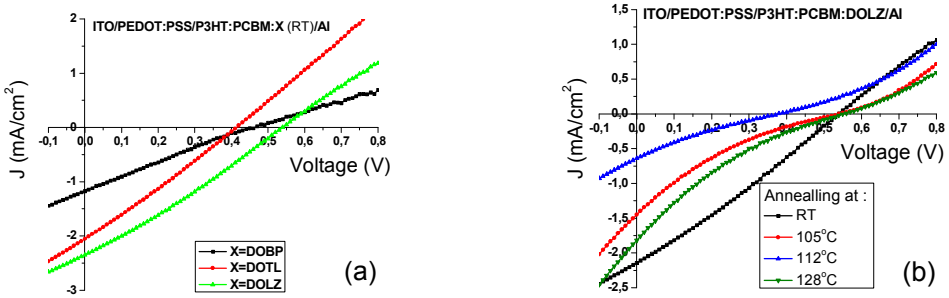

Figure 5. J-V characteristics (under AM1.5G-simulated solar illumination of 100 mW/cm^2) of the investigated polymer solar cells: (a) with organic compounds used as functional additives to the active layer at room temperature (RT) and (b) of the specific active layer P3HT:PCBM:**DOLZ** at indicated temperatures.

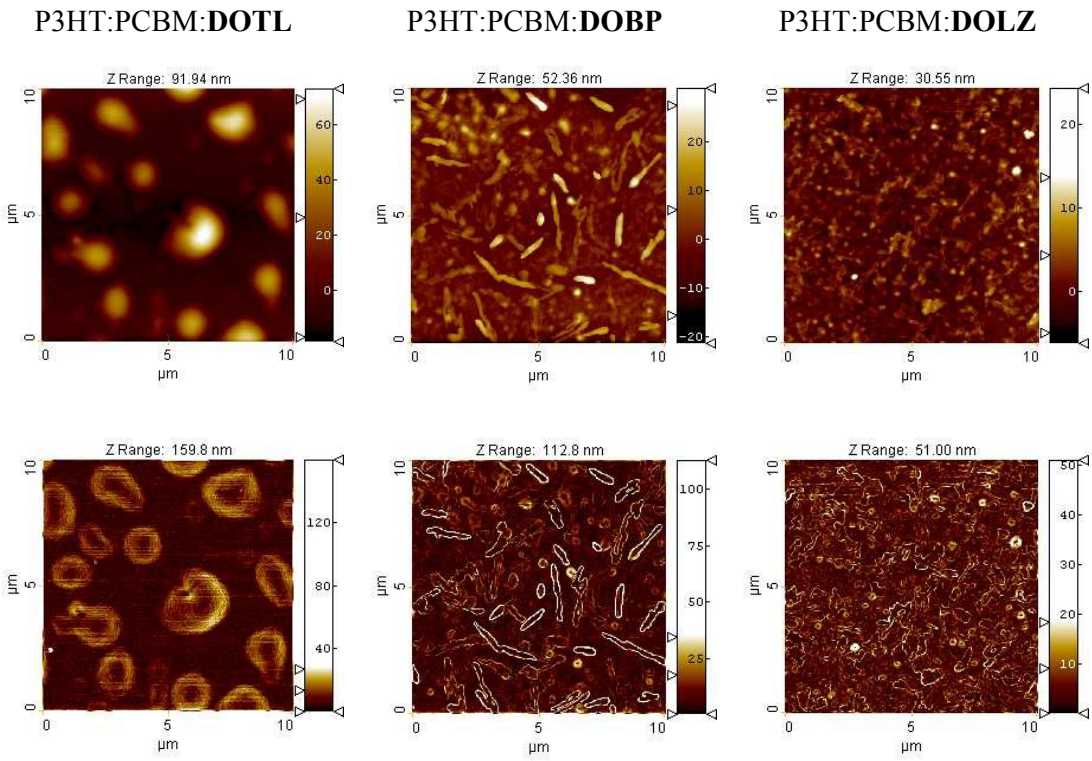

Figure 6. AFM images of P3HT:PCBM:**X** resulting mixtures, where X=**DOTL** (S_a = 12.83 nm, S_q = 16.77 nm), X=**DOBP** (S_a = 4.21 nm, S_q = 5.74 nm) and X=**DOLZ** (S_a = 1.86 nm, S_q = 2.39 nm), respectively: topography (top row) and Sobel transformation (bottom row).

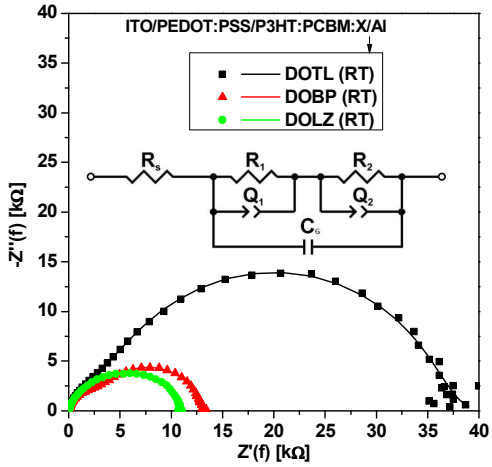

Figure 7. Impedance Nyquist plots of ITO/PEDOT:PSS/P3HT:PCBM:**X**/Al BHJ devices (with active layer non-annealed) along with fit results and an equivalent circuit of the devices (R_S represents the series resistance, C_G capacitance between anode and cathode, R is resistance and Q is constant phase element of the investigated layer).

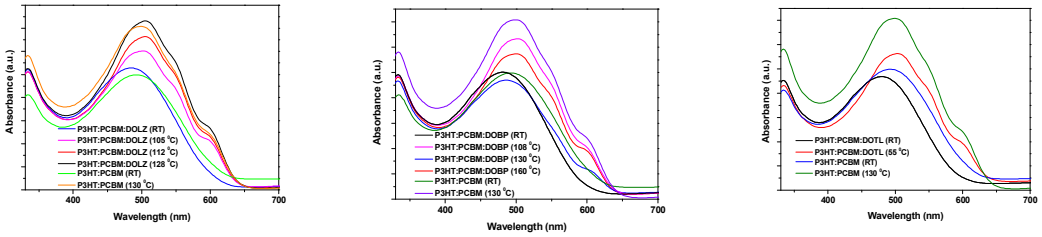

Figure 8. UV-Vis absorption spectra of P3HT:PCBM:**X** measured on films before and after thermal annealing as indicated.

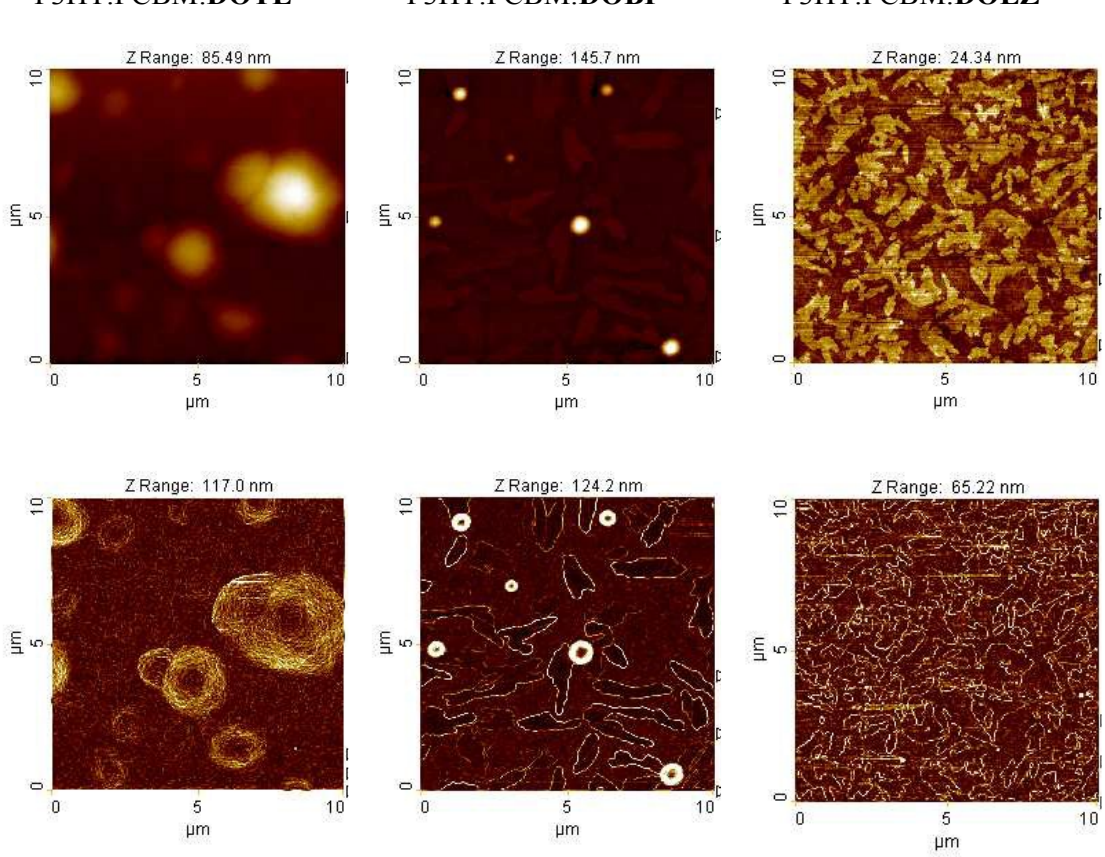

Figure 9. AFM images of P3HT:PCBM:**X** at various temperature of active layer annealing, where X: **DOTL** at 55 °C (S_a = 8.86 nm, S_q = 12.88 nm), **DOBP** at 160 °C (S_a = 4.92 nm, S_q = 9.59 nm) and **DOLZ** at 128 °C (S_a = 1.78 nm, S_q = 2.08 nm)**,** respectively: topography (left side) and Sobel transformation (right side)

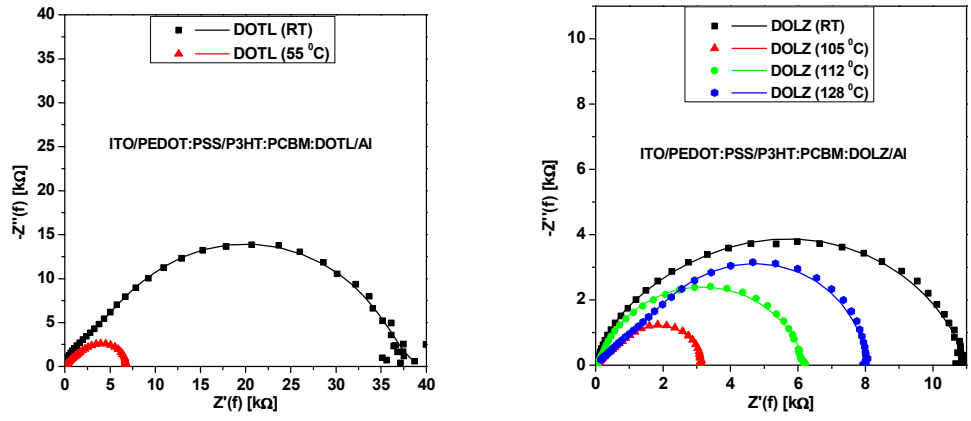

Figure 10. Impedance Nyquist plots of ITO/PEDOT:PSS/P3HT:PCBM:**X**/Al BHJ devices (with active layer annealed at different temperatures)

Table 4. Main photovoltaic characteristics of BHJ devices doped with **DOTL**, **DOBP** and **DOLZ** compounds.

Active layer	T [^{o}C]	J_{sc} [mA/cm^2]	V_{oc} [V]	FF [-]	PCE [%]	P_{max} [μW]
P3HT:PCBM:**DOTL**	RT	1.86	0.517	0.26	0.25	13.7
	55	2.20	0.548	0.19	0.24	18.5
P3HT:PCBM:**DOBP**	RT	1.16	0.494	0.21	0.12	6.96
	108	0.19	0.329	0.20	0.01	0.80
	130	0.47	0.417	0.19	0.04	2.13
	160	1.43	0.493	0.15	0.10	5.37
P3HT:PCBM:**DOLZ**	RT	2.23	0.540	0.28	0.34	17.0
	105	1.47	0.534	0.17	0.14	7.40
	112	0.44	0.315	0.21	0.03	2.16
	128	1.55	0.552	0.17	0.14	7.63

Notes: V_{oc} - open circuit voltage. J_{sc} - short circuit current density. FF - fill factor. PCE - power conversion efficiency. P_{max} – the maximum power of the pixel with PCE_{max} RT – room temperature.

Table 5. Relaxation times (τ_1 and τ_2) of devices with active layer annealed at indicated temperatures (T) under illumination.

Active layer	T, [°C]	τ_1, [μs]	τ_2, [μs]
P3HT:PCBM:**DOTL**	RT	32.71	102.7
	55	10.69	70.92
P3HT:PCBM:**DOBP**	RT	0.52	58.95
	108	2.73	249.2
	130	32.62	279.9
	160	113.4	146.9
P3HT:PCBM:**DOLZ**	RT	0.40	16.31
	105	14.00	110.3
	112	1.210	137.8
	128	12.71	85.85

Graphical Abstract